Received: 2 December 2021 | Revised: 19 January 2022 | Accepted: 19 January 2022

DOI: 10.1002/poc.4333

RESEARCH ARTICLE

Journal of Physical Organic Chemistry WILEY

On the mechanism of the Au(I)-mediated addition of alkynes to anthranils to furnish 7-acylindoles

Ioannis Stylianakis[1] | **Iraklis Litinas**[1] | **Olalla Nieto Faza**[2] | **Antonios Kolocouris**[1] | **Carlos Silva López**[2]

[1]Department of Medicinal Chemistry, Faculty of Pharmacy, National and Kapodistrian University of Athens Panepistimioupolis Zografou, Athens, Greece

[2]Departamento de Química Orgánica, Universidad de Vigo, Campus Lagoas-Marcosende, Vigo, Spain

Correspondence
Antonios Kolocouris, Department of Medicinal Chemistry, Faculty of Pharmacy, National and Kapodistrian University of Athens Panepistimioupolis Zografou, Athens 15771, Greece.
Email: ankol@pharm.uoa.gr

Carlos Silva López, Departamento de Química Orgánica, Universidad de Vigo, Campus Lagoas-Marcosende, 36310 Vigo, Spain.
Email: carlos.silva@uvigo.es

Funding information
Xunta de Galicia, Grant/Award Number: ED431C 2021/41; Ministerio de Ciencia e Innovación, Grant/Award Number: PID2020-115789GB-C22; Chiesi Hellas

Abstract

Indole is a very common structural motif in alkaloids with a remarkable history in pharma industry. In the continuous search for more direct and efficient access to these valuable structures, a new and rather elegant approach was found by Jin and coworkers, which involved a gold(I)-mediated addition of alkynes onto anthralins. This approach selectively furnishes 7-acylindoles in a rather expeditious way, and it has been shown to be compatible with a large range of decorated reactants, both at the alkyne side and at the anthralin side. We studied the mechanism of this reaction with a set of different alkynes, including disubstituted ones, to establish similarities and differences between them and to aid in the elucidation of key steps in the reaction pathway. The observed regioselectivity seems to be connected to the irreversible formation of a key α-imino gold carbene intermediate, common to all reaction profiles, through the initial regioselective nucleophilic attack of the anthranil N atom onto the alkyne fragment.

KEYWORDS

alkynyl activation, gold catalysis, α-imino gold carbene

1 | INTRODUCTION

Indoles are a prominent class in the alkaloid superfamily of organic compounds. They are also common structural motifs in an ever-increasing range of pharmaceuticals, aimed to treat diseases as diverse as cancer, asthma, various types of microbial infections, or depression.[1] Within this class of compounds, 7-acyl-indoles are also a valuable building block for bioactive compounds.[2–4] In order to add another alternative to the organic chemist toolbox for the preparation of 7-acyl-indoles, Jin and coworkers developed an elegant synthetic method employing a gold(I)-catalyzed C–H annulation of anthralins with terminal alkynes, initially using ynamides with benzyl and mesylate substituents (e.g., BnN(Ms)≡CH), but later also including non-polarized terminal alkynes or disubstituted alkynes (Scheme 1).[5] This methodology has recently become quite attractive for the synthesis of N-doped polyaromatic

Dedicated to Prof. Barry Carpenter, brilliant as a chemist and admirable as a fellow human being.

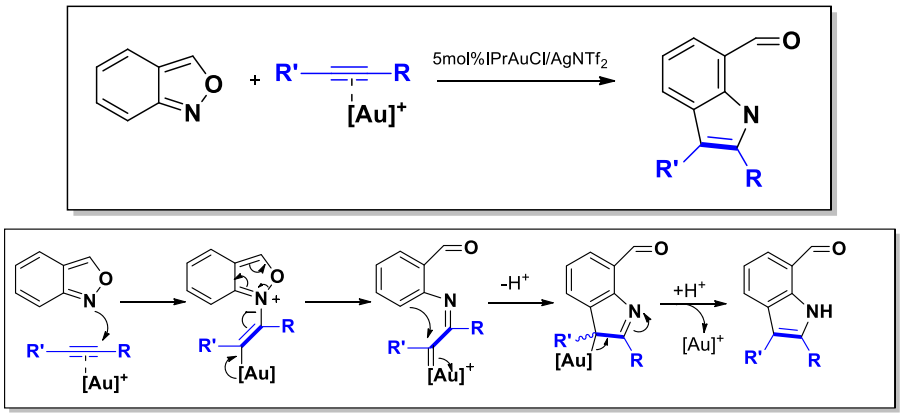

SCHEME 1 Annulation of anthranil with alkynes using IPrAuCl/AgNTf2 as preferred catalyst (top). Suggested basic mechanistic steps for the C–H annulation of anthralins with terminal alkynes (bottom)[5]

hydrocarbons (PAHs), where an *o*-ethynylbiaryl system is made to react with the anthranil fragment.[6] A general outline of the plausible reaction mechanism included the attack of the nitrogen nucleophile to one of the alkyne carbon atoms, generating an α-imino gold carbene intermediate as depicted in Scheme 1 (bottom). The participation of these α-imino gold carbene complexes as reaction intermediates has emerged as an attractive field in the synthesis of nitrogen heterocycles.[7–11]

Our interest in gold catalysis in general and gold carbene generation in particular prompted us to carry out a thorough investigation of the reaction mechanism of this promising synthetic procedure. We therefore explored the mechanism of this reaction between anthralins and a set of different alkynes to elucidate key steps in the reaction pathway. We investigated the regioselectivity with ynamides and terminal alkynes, which selectively provide the 2- compared with the 3-substituted 7-acyl-indole ring, and further expanded our analysis to the less trivial asymmetric disubstituted alkynes, for which, surprisingly, only one regioisomer is also observed in the original experimental work.[5] The results of such an investigation also shed light onto the mechanistic machinery for this reaction, and they uncover details about the catalyst, the reaction conditions employed, and the role of the α-imino gold carbene intermediate.

2 | RESULTS AND DISCUSSION

For the reaction of anthralin with the gold-activated triple bond, we anticipated a mechanism consisting of six steps. There are two alternatives for the initial nucleophilic attack onto the triple bond (Scheme 2), where regioselectivity is determined: The nitrogen atom of the oxazole ring can attack the gold-polarized triple bond at C-1 (Path 1) or C-2 (Path 2) to generate intermediates 3n2 or 3n1, respectively. The second step involves an interesting redistribution of π-electrons resulting in the cleavage of the N–O bond to form 4n2 (path 2) or 4n1 (path 1). Then, an electrophilic aromatic substitution reaction occurs between the electron deficient carbon of the α-imino gold carbene and the phenyl fragment resulting in intermediates 5n2 or 5n1, which can have an *anti* or *syn* relative orientation of the hydrogen atoms attached to the bond forming carbons (Scheme 2). The fourth and fifth steps comprise proton migrations such that ring aromaticity is recovered at the phenyl unit (6n2 or 6n1, respectively), and the sixth step includes the deauration and concomitant aromatization of the pyrrole ring to form isomeric 7-acylindoles 7n2 or 7n1, respectively. The product obtained in the experiment is 7n2 with the substituent on the reacting alkyne installed at 2- instead of the 3-carbon of the 7-acyl-indole ring.

2.1 | Reaction between anthranil and a benzyl-substituted ynamide

We calculated the two paths described in Scheme 2 for the reaction of anthranil (2a in reference[5]) with ynamide BnN(Ms)C≡CH (1a in reference[5]), in which the triple bond is polarized because of the adjacent NMs group to the triple bond carbon as described in Scheme 3. We used in our calculations a simpler ylide (see Scheme 3) as model of the catalyst IPrAuCl/AgNTf2 used by Jin et al.[5]

For the nucleophilic attack of the anthranil nitrogen onto the triple bond, we calculated an energy difference of 14.9 kcal/mol between TS_{3a1} versus TS_{3a2}, in favor of the attack to the internal, more polarized, alkyne carbon, which ultimately leads to 7a2, which is the experimentally observed product. The 9.8 kcal/mol barrier for the attack at C-2 is consistent with the low thermal requirements of this process (−20°C; see Table 1). The structure TS_{3a2} may be additionally stabilized because of the cooperative π-donating character of two geminal nitrogen

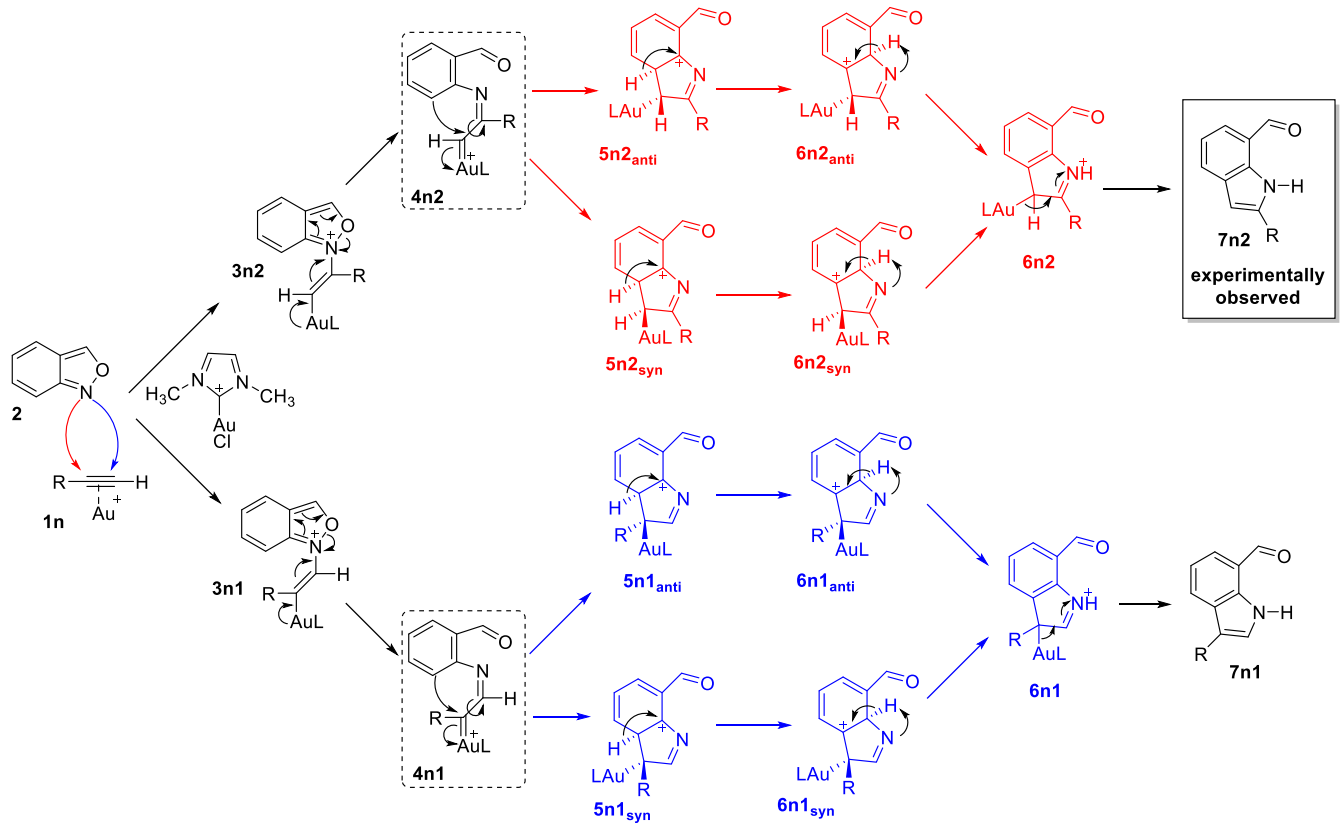

SCHEME 2 Regioselectivity models description for the mechanism of the reaction of a terminal alkyne with anthranil. The key α-imino gold carbene intermediate is highlighted with a dashed-line frame

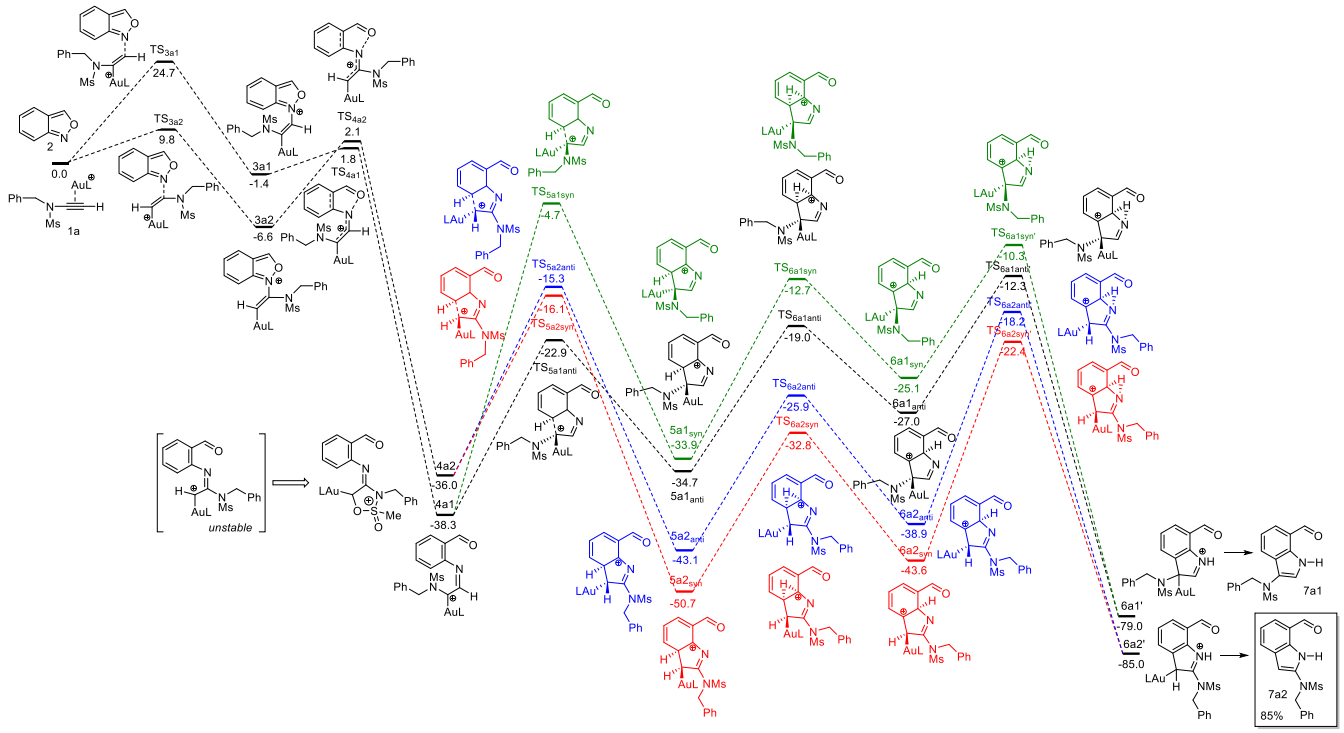

SCHEME 3 Reaction between anthranil and the ynamide BnN(Ms)≡CH. Relative Gibbs energies (kcal/mol, 298 K and 1 atm). From the α-imino gold carbene intermediate, blue and red colors indicate the two regioselectively favorable paths whereas black and green are used for the disfavored nucleophilic attack

TABLE 1 Calculated activation Gibbs energies (kcal/mol) for each step of the mechanism between anthranil and different alkynes, that is, BnN(Ms)C≡CH (3a series), cypC≡CH (3b series), PhC≡CPh (3c series), and PhC≡CBu (3d series)

1st step	$\Delta G^{\ddagger}$	2nd step	$\Delta G^{\ddagger}$	3rd step	$\Delta G^{\ddagger}$	4th step	$\Delta G^{\ddagger}$	5th step	$\Delta G^{\ddagger}$
TS_{3a1}	24.7	TS_{4a1}	3.2	$TS_{5a1anti}$	15.4	$TS_{6a1anti}$	15.7	$TS_{6a1anti'}$	14.7
				TS_{5a1syn}	33.6	TS_{6a1syn}	21.2	$TS_{6a1syn'}$	14.8
TS_{3a2}	9.8	TS_{4a2}	8.7	$TS_{5a2anti}$	20.7	$TS_{6a2anti}$	17.2	$TS_{6a2anti'}$	20.7
				TS_{5a2syn}	19.9	TS_{6a2syn}	17.9	$TS_{6a2syn'}$	21.2
TS_{3b1}	16.2	TS_{4b1}	4.7	$TS_{5b1anti}$	4.6	$TS_{6b1anti}$	10.1	$TS_{6b1anti'}$	15.4
				TS_{5b1syn}	12.5	TS_{6b1syn}	16.3	$TS_{6b1syn'}$	18.7
TS_{3b2}	10.7	TS_{4b2}	9.6	$TS_{5b2anti}$	0.5	$TS_{6b2anti}$	15.6	$TS_{6b2anti'}$	18.6
				TS_{5b2syn}	0.0	TS_{6b2syn}	15.3	$TS_{6b2syn'}$	14.7
TS_{3c}	12.3	TS_{4c}	6.9	TS_{5canti}	14.5	TS_{6canti}	17.2	$TS_{6canti'}$	16.5
				TS_{5csyn}	9.8	TS_{6csyn}	15.8	$TS_{6csyn'}$	17.9
TS_{3d1}	13.1	TS_{4d1}	7.0	$TS_{5d1anti}$	14.9	$TS_{6d1anti}$	18.6	$TS_{6d1anti'}$	17.7
				TS_{5d1syn}	8.8	TS_{6d1syn}	13.5	$TS_{6d1syn'}$	15.9
TS_{3d2}	13.9	TS_{4d2}	7.9	$TS_{5d2anti}$	8.7	$TS_{6d2anti}$	15.2	$TS_{6d2anti'}$	17.3
				TS_{5d2syn}	5.4	TS_{6d2syn}	15.0	$TS_{6d2syn'}$	15.3

atoms versus one nitrogen atom at each end of the triple bond in TS_{3a1}. This interaction has geometrical consequences at both the pair of transition states and also the subsequent intermediates 3a1 and 3a2. For instance, the orientation of the amine group is drastically different in these two transition states (see Figure 1). In TS_{3a1}, the amine lies co-planar to the entering nucleophile and its lone pair is therefore orthogonal and non-interacting in the process. In TS_{3a2}, however, this lone pair is conjugated with the π-electrons participating in the reaction. The C-NMs bond length is diagnostic for this pi-donating interaction (1.36 vs. 1.31 Å in TS_{3a1} vs. TS_{3a2}) as well as the triple C–C bond (1.27 vs. 1.29 Å in TS_{3a1} vs. TS_{3a2}). The regioselectivity of 2- over 3-position of the final amino-substituted 7-acyl-indole ring is decided at this first transition state because the energy difference between the competing TS_{3a1} and TS_{3a2} is very large and the subsequent step involves an irreversible energy cliff. This irreversible step involves what looks like an interesting pseudopericyclic electrocyclic ring opening (vide infra).[12]

The pseudopericyclic nature of this reaction justifies the very meager energy demands in both paths (less than 10 kcal/mol). Additionally, the associated exergonicity of the process is enhanced by the recovery of aromaticity at the phenyl fragment. This conversion from an orthoquinone-like structure into an *o*-formyl aniline fragment is the driving force of the catalytic cycle with an energy drop of about 40 kcal/mol, leading to α-imino gold intermediates 4a1 and 4a2.

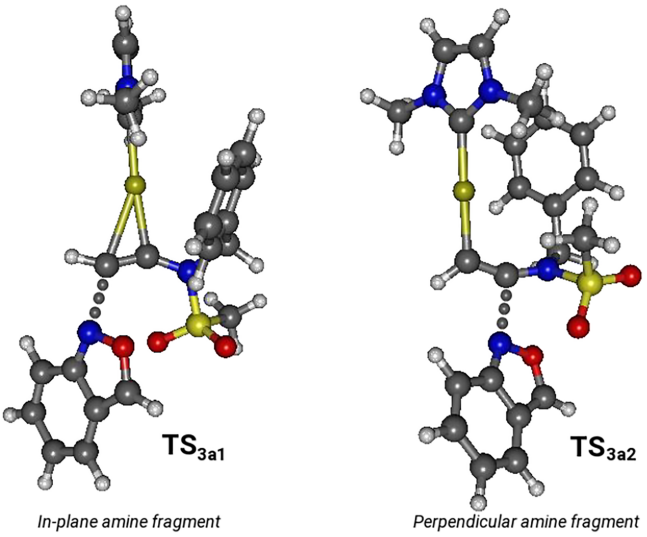

FIGURE 1 Side by side comparison of transition states TS_{3a1} and TS_{3a2}. In the latter, geometrical evidence suggests the participation of the lone pair at the ynamide nitrogen in the stabilization of the resulting structure through conjugation to the alkyne. The Au bonding is also indicating a more advanced transition state in TS_{3a2}

Onto these intermediates, an electrophilic aromatic substitution takes place via the gold-activated carbon atom. Two possible approaches, *anti* or *syn*, are viable for this step. In the case of the favored intermediate 4a2, both approaches are almost equally probable, given the similarity of their energy requirements (about 22 kcal/

mol). The intramolecular character of this S_EAR involves the formation of isomeric fused systems 5a1 and 5a2 in their *anti* and *syn* configurations. Two sequential proton migrations allow again full recovery of the aromaticity lost in the S_EAr step and furnish the final gold-activated compounds, 7a1 and 7a2, which are released upon de-auration (probably through a ligand exchange step involving the starting alkyne 1a to reinitiate the catalytic cycle).

2.2 | Reaction between anthranil and an alkyl-substituted terminal alkyne

The barriers for the two alternative nucleophilic attacks of the anthranil nitrogen onto the gold(I)-activated triple bond are much closer than in system 1a. The activation energies are 16.2 and 10.7 kcal/mol for terminal versus internal attack (Scheme 4; compared with 24.7 and 9.8 kcal/mol in system *a*, Scheme 3). These closer values are due to the less extreme electron donating effect of the alkyl compared with the amine group. The 5.5 kcal/mol energy difference is still enough to obtain complete regioselectivity under the operating reaction conditions. In this occasion, the apparent pseudopericyclic ring opening is still showing low energy demands (less than 10 kcal/mol), but it is not nearly as exergonic (about 10 kcal/mol of product stabilization in this case vs. ∼30 kcal/mol when an inamide was the reacting counterpart). This difference is attributed to the less stabilized carbocations 4b1 and 4b2 when an alkyl group is all there is to donate charge onto the electron density depleted carbon atom. As a consequence of these unstable carbocations, the S_EAR reaction becomes kinetically much faster and it also turns itself into the driving force of the catalytic process, with an associated energy drop of about 30 kcal/mol. The two steps between the initial nucleophilic attack and this energy cliff are mildly exergonic and kinetically fast, with small associated barriers. This also provides a scenario where the initial attack must be regioselectivity determining because reversion at the first two pairs of intermediates (3b1, 3b2 and 4b1, 4b2) is unlikely. Two proton migration steps, analogous to those already observed with the ynamide reaction, provide the final 7-acyl-indole isomers 7b1 and 7b2.

For this reaction, we decided to explore in more depth the second step, for which the molecular topology suggests that a pseudopericyclic transformation may be taking place. For this, we computed nucleus-independent chemical shifts (NICS) on two axes perpendicular to the

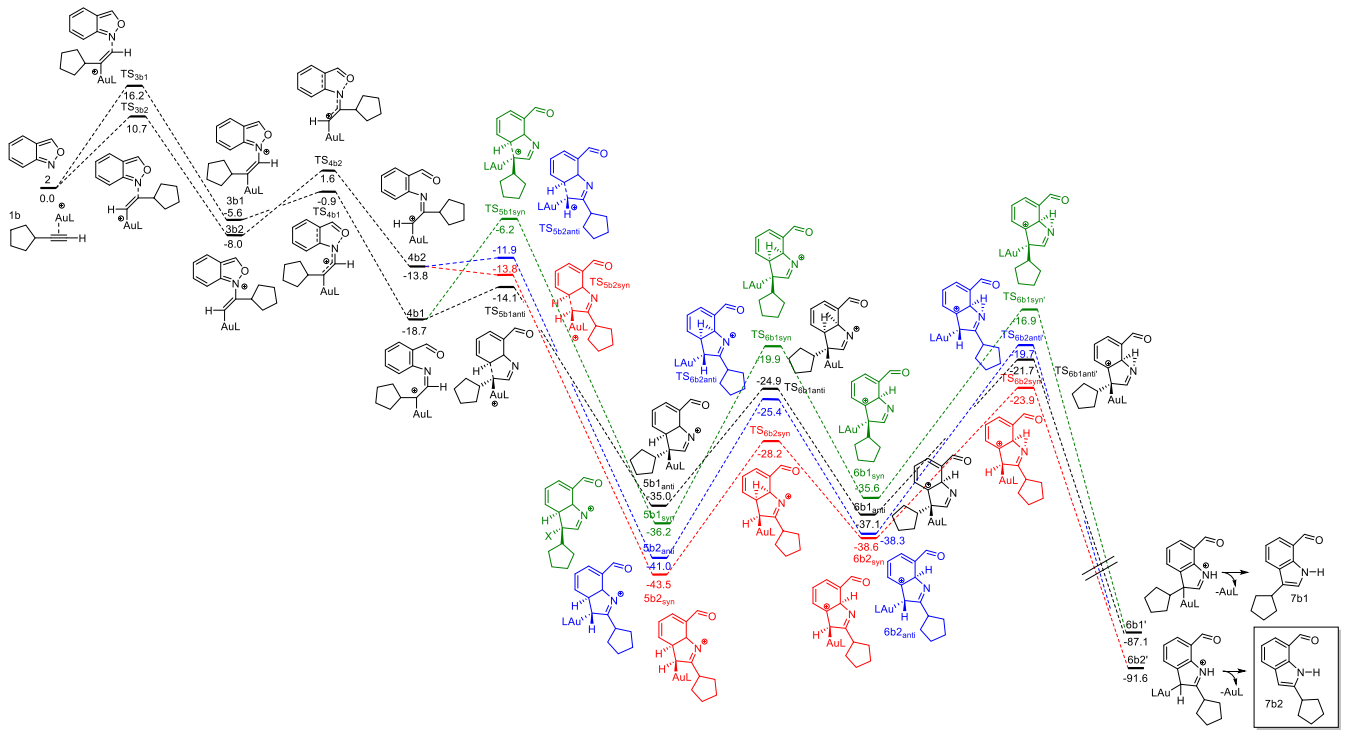

SCHEME 4 Reaction of anthranil with an alkyl-substituted alkyne. Relative Gibbs energies (kcal/mol, 298 K and 1 atm). From the α-imino gold carbene intermediate, blue and red colors indicate the two regioselectively favorable paths whereas black and green are used for the disfavored nucleophilic attack

phenyl and azole fragments in the anthranil moiety (see Figure 2). Our results showed the obvious aromatic profile at the phenyl fragment, which is strongly conserved when going from the transition state (TS_{4b2}) into the reaction intermediate (4b2). On the azole ring however, aromaticity is lost in this step. Losing aromaticity is not really surprising in this step, because the azole ring is being opened, but the fact that mild aromaticity is present at the transition state is in contradiction with a fully pseudopericyclic process. The relatively mild aromaticity at this transition state and its maximum value at the molecular plane suggests that part of this aromaticity may be due to the sigma skeleton and perhaps this step lays in a gray area between peri- and pseudopericyclic mechanisms.[13]

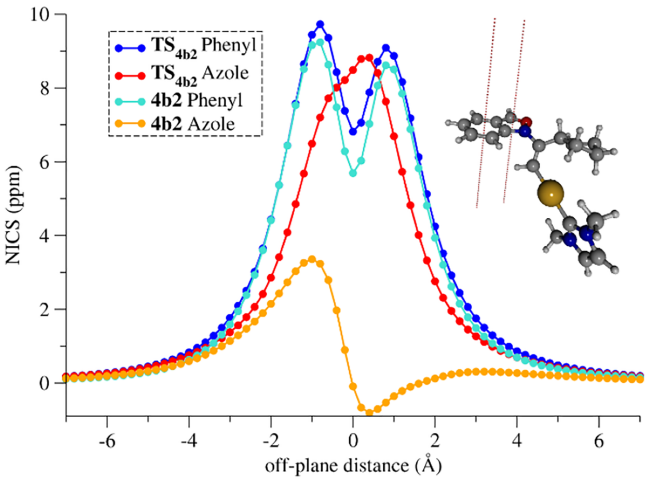

FIGURE 2 Nucleus-independent chemical shifts (NICS) computed along two axes perpendicular to the anthranil heterocycle at TS_{4b2} and 4b2. The axes employed are illustrated in the molecular geometry

2.3 | Reaction between anthranil and diphenyl acetylene

In the case of the symmetrically substituted diphenyl acetylene, our calculations show a similar profile to those discussed above. In this case, the starting barrier is 12.3 kcal/mol, again, not as low as with the ynamide due to the reduced donating capabilities of the phenyl fragment. The pseudopericyclic ring opening is also strongly exergonic (about 20 kcal/mol; Scheme 5) because the carbocation is stabilized by the adjacent phenyl ring. In this case, the presence of two phenyl rings at the ends of the alkyne fragment pays dividends on the reaction profile because one phenyl substituent acts in the stabilization of the initial transition state, TS_{3c}, and the other phenyl ring allows for the stabilization of the carbocation after the

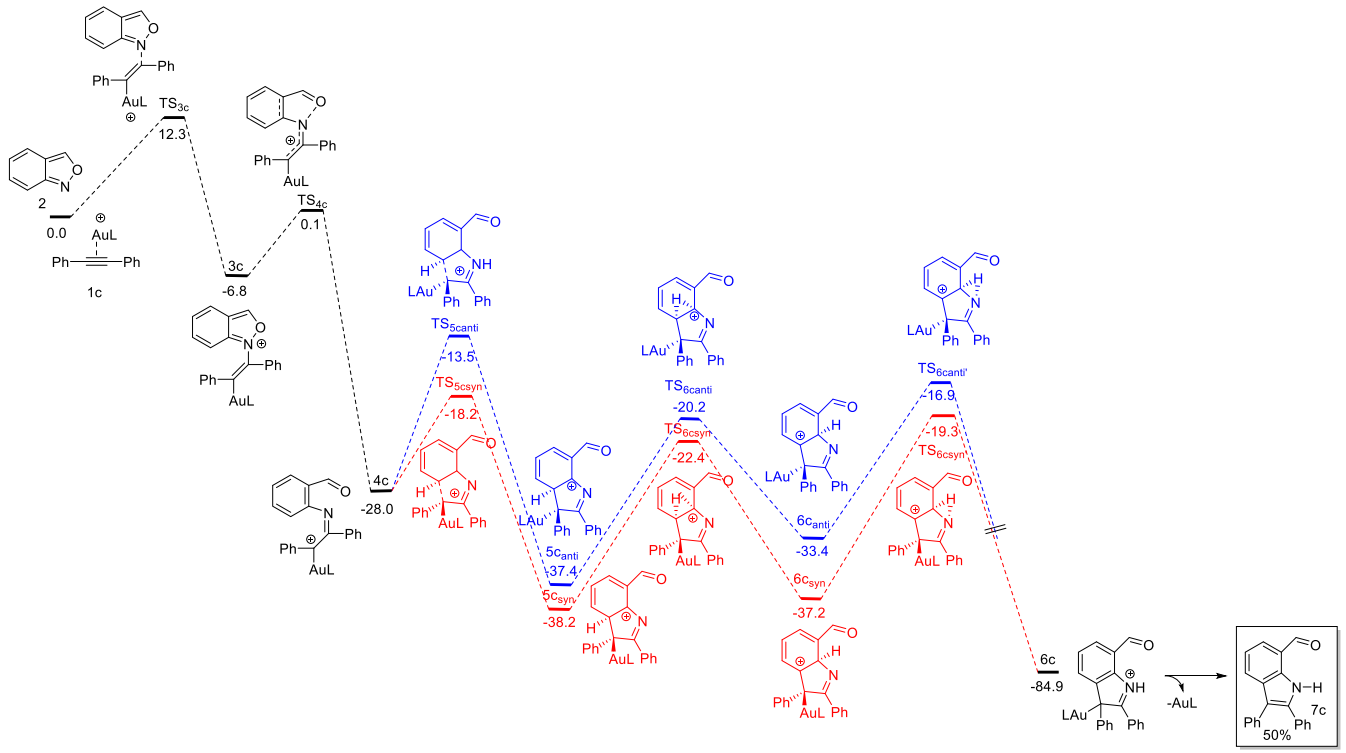

SCHEME 5 Reaction of anthranil with diphenyl acetylene. Relative Gibbs energies (kcal/mol, 298 K and 1 atm)

N–O bond cleavage (4c). The subsequent electrophilic aromatic substitution is more favorable through the *syn* approach and involves only a barrier of 10 kcal/mol. Then again, two proton migration steps allow for recovery of the aromaticity and the release of the experimentally observed 2,3-diphenyl 7-acylindole 7c.

2.4 | Reaction between anthranil and non-symmetrically substituted internal alkynes

Finally, for the case of non-symmetrical alkyl/phenyl alkynes, we chose to use phenyl and *n*-butyl substituents to illustrate the case (Scheme 6). The activation energy for the initial attack at the aromatic or aliphatic sides of the triple bond is similar, differing only by 0.8 kcal/mol. The subsequent N–O bond cleavage features a small barrier and precedes a significant energy drop of about 25 kcal/mol. This situation therefore suggests that both regioisomers could be formed in this process, because the difference in energy barriers for the rate-limiting step is so shallow. Once intermediates 4d1 and 4d2 are formed, the same sequence of events described for all the previous cases operate: cyclization via a S_EAr step, two hydrogen migrations to recover aromaticity after the S_EAr, and gold decomplexation to furnish the final indole.

Experimentally, this mode of alkyne substitution was not broadly tested, but in the few cases that it was, the reaction behaved regioselectivity by furnishing only the 2-alkyl, 3-aryl indole analogous to 7d1 in Scheme 6. Interestingly, however, the reaction yield is significantly lower than those observed with other kind of alkynes. Jin et al. hypothesized that perhaps the 3-aryl, 2-alkyl indole is not observed due to a competitive hydrogen migration occurring at 4d2, which may obstruct the S_EAr step. We therefore decided to explore whether such possibility may be indeed competitive and become a deleterious effect on this reaction path. Indeed, a 1,2-H migration step, very similar to other found and described in our group in the past, could be located and found to be competitive with the cyclization via S_EAr when the alkyl group is directly attached to the gold carbene. We computed the transition state for this migration lying only 1.2 kcal/mol above TS_{5d2syn}.

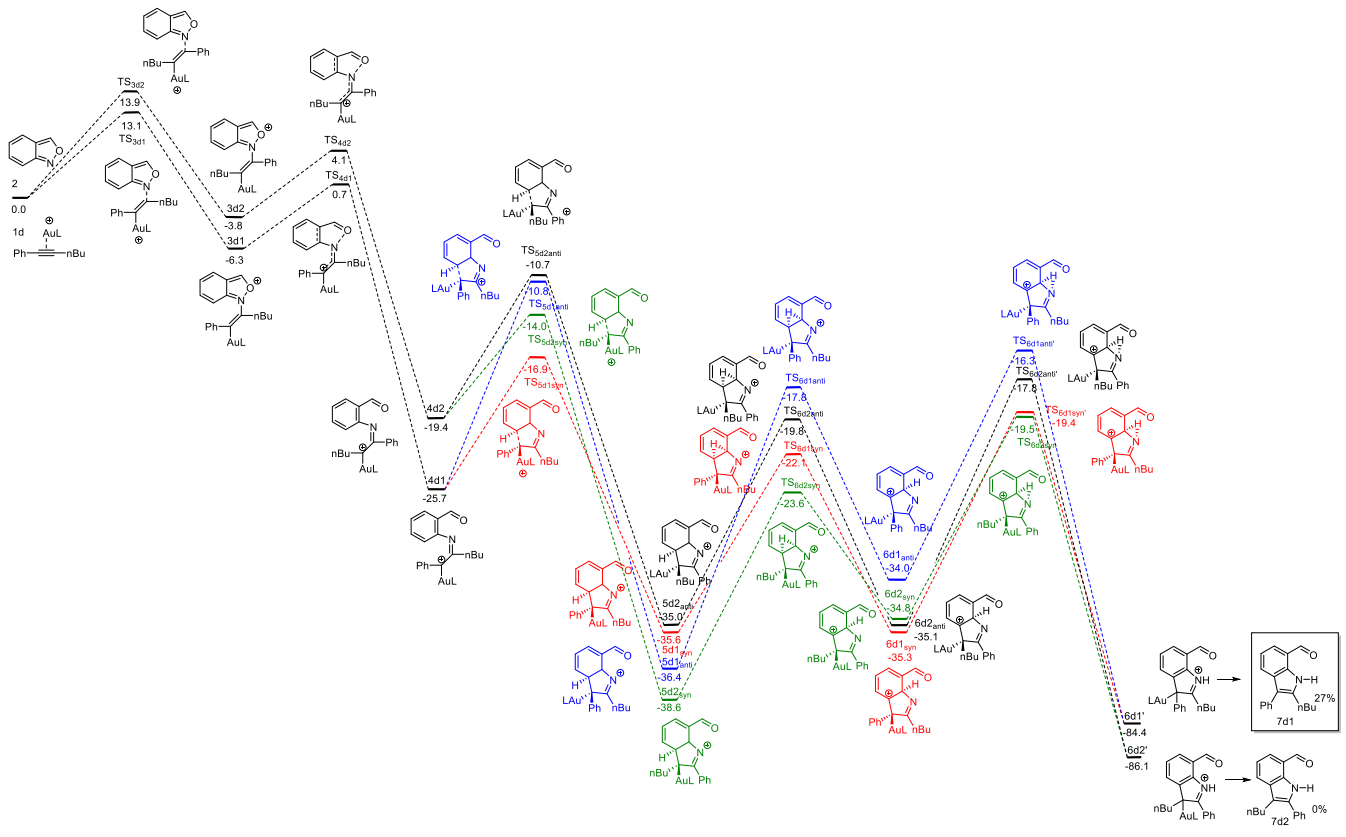

SCHEME 6 Reaction of anthranil with an unsymmetrical disubstituted alkyne. Relative Gibbs energies (kcal/mol, 298 K and 1 atm). From the α-imino gold carbene intermediate, blue and red colors indicate the two regioselectively favorable paths whereas black and green are used for the disfavored nucleophilic attack

In general, the same main mechanistic features apply to all the alkynes considered. The reaction is initiated with a nucleophilic attack, which is also regioselectivity determining. This attack is preferentially directed onto the internal carbon atom of the alkyne, and the preference is more pronounced the more polarized the alkyne in the starting substrate. In doubly substituted triple bonds, the preference is less marked, but it seems to favor the attack onto the alkyl-substituted versus aryl-substituted carbon atoms. The N–O bond cleaves in an apparent pseudopericyclic step that is not energy demanding, but it precedes an energy drop that makes the process irreversible. The open intermediate thus obtained undergoes cyclization via a S_EAR of the α-imino gold carbene onto the phenyl fragment. A hydrogen rearrangement in two steps recovers the aromaticity of the bicyclic system and furnishes the final 7-acylindole. The main differences found among the various alkynes tested are the starting barrier for the nucleophilic attack, which depends on the polarization of the triple bond and the energy drop after the N–O bond cleavage, which ranges from −35 to −13 kcal/mol, also depending on the nature of the starting alkyne and its ability to stabilize the forming α-imino gold carbene. The rate-limiting step is found at the late rearomatization stage of the mechanism of the regio-favored pathways, but in the disfavored ones, the starting nucleophilic attack may also be rate limiting (Table 1).

3 | CONCLUSION

In this work, we studied the in situ gold(I)-catalyzed generation of α-imino gold carbene intermediates en route from anthralin and a range of alkynes to 7-acyl-indoles. They are shown to be key intermediates that further evolve via a S_EAr mechanism unless migrating hydrogens can be found at Cα (primary or secondary alkyl substituents), in which case a 1,2-H migration seems to become competitive with the electrophilic aromatic substitution.

We showed that the observed regioselectivity is decided at the initial nucleophilic attack of the anthranil nitrogen onto the alkyne fragment because the formation of the α-imino gold carbene intermediate is an irreversible step. The nature of the substituents at the alkyne fragment is key to determine (1) the degree of selectivity, (2) the height of the initial and rate-limiting barrier, and (3) the energy drop associated to the formation of the α-imino gold carbene. It is worth noting that Au(III) species also catalyze a similar transformation, although the final outcome seems strongly dependent on the counterion chaperoning gold.[6,14,15]

4 | COMPUTATIONAL SECTION

Throughout this work, the Kohn–Sham formulation of density functional theory was employed.[16] The meta-hybrid density functional M06[17] has been used with the extended double-ζ quality def2-SVPP basis set for all the static calculations. This combination of density functional and basis set has been found to provide good performance in homogeneous gold catalysis.[18,19] All geometry optimizations have been carried out using tight convergence criteria and a pruned grid for numerical integration with 99 radial shells and 590 angular points per shell. In some challenging cases, this grid was enlarged to 175 radial shells and 974 points per shell for first row atoms and 250 shells and 974 points per shell for heavier elements. These challenging optimizations are usually associated with very soft vibrational modes (usually internal rotations). Analysis of the normal modes obtained via diagonalization of the Hessian matrix was used to confirm the topological nature of each stationary point. The wavefunction stability for each optimized structure has also been checked.[20] Solvation effects have been taken into account variationally throughout the optimization procedures via the polarizable continuum model (PCM)[21] using parameters for toluene and taking advantage of the smooth switching function developed by York and Karplus.[22] Concerning the structures involved in these simulations, we simplified the cationic gold complex employed in the experimental work (complex A) using 1,3-bis-methyl-imidazol-2-ylidene gold as a simpler model of the catalyst IPrAuCl/$AgNTf_2$ in order to find a balance between accuracy and computational efficiency. All the calculations performed in this work have been carried out with the Gaussian 09 program.[23]

ACKNOWLEDGMENTS

This research includes part of the PhD work of IS. AK thanks Chiesi Hellas for supporting this research. CSL thanks the Ministerio de Ciencia e Innovación (PID2020-115789GB-C22) and Xunta de Galicia (ED431C 2021/41), which partially funded this work. Generous allocation of supercomputer resources by CESGA is also acknowledged.

DATA AVAILABILITY STATEMENT

Data supporting the findings of this study can be found in the supporting information of this article.

ORCID

Antonios Kolocouris https://orcid.org/0000-0001-6110-1903

Carlos Silva López https://orcid.org/0000-0003-4955-9844

REFERENCES

[1] a) J. Dhuguru, R. Skouta, *Molecules* **2020**, *25*, 1615A; b) N. Chadha, O. Silakari, *Eur. J. Med. Chem.* **2017**, *134*, 159; c) A. Kumari, R. K. Singh, *Bioorg. Chem.* **2019**, *89*, 103021; d) H. A. Hamid, A. N. Ramli, M. M. Yusoff, *Front. Pharmacol.* **2017**, *8*, 96.

[2] M. P. Moyer, J. F. Shiurba, H. Rapoport, *J. Org. Chem.* **1986**, *51*, 5106.

[3] T. Barf, F. Lehmann, K. Hammer, S. Haile, E. Axen, C. Medina, J. Uppenberg, S. Svensson, L. Rondahl, T. Lundbäck, *Bioorg. Med. Chem. Lett.* **2009**, *19*, 1745.

[4] J. A. Nieman, S. K. Nair, S. E. Heasley, B. L. Schultz, H. M. Zerth, R. A. Nugent, K. Chen, K. J. Stephanski, T. A. Hopkins, M. L. Knechtel, N. L. Oien, J. L. Wieber, M. W. Wathen, *Bioorg. Med. Chem. Lett.* **2010**, *20*, 3039.

[5] H. Jin, L. Huang, J. Xie, M. Rudolph, F. Rominger, A. S. K. Hashmi, *Angew. Chem. Int. Ed.* **2016**, *55*, 794.

[6] Z. Zeng, H. Jin, K. Sekine, M. Rudolph, F. Rominger, A. S. K. Hashmi, *Angew. Chem. Int. Ed.* **2018**, *57*, 6935.

[7] E. Aguilar, J. Santamaría, *Org. Chem. Front.* **2019**, *6*, 1513.

[8] R. Dorel, A. M. Echavarren, *Chem. Rev.* **2015**, *115*, 9028.

[9] X. Tian, L. Song, A. S. K. Hashmi, *Chem. A Eur. J.* **2020**, *26*, 3197.

[10] K. Vipin Raj, P. S. Dhote, K. Vanka, C. V. Ramana, *Front. Chem.* **2021**, *9*, 689780.

[11] F. F. Mulks, *Gold Bull.* **2022**, 1. https://doi.org/10.1007/s13404-021-00298-1

[12] a) C. S. López, O. N. Faza, M. Freindorf, E. Kraka, D. Cremer, *J. Org. Chem.* **2016**, *81*, 404; b) R. Villar López, O. Nieto Faza, E. Matito, C. Silva López, *Org. Biomol. Chem.* **2017**, *15*, 435; c) C. S. López, O. N. Faza, F. P. Cossío, D. M. York, A. R. de Lera, *Chem. A Eur. J.* **2005**, *11*, 1734; d) W. M. F. Fabian, V. A. Bakulev, C. O. Kappe, *J. Org. Chem.* **1998**, *63*, 5801; e) D. M. Birney, *J. Org. Chem.* **1996**, *61*, 243; f) S. Ham, D. M. Birney, *J. Org. Chem.* **1996**, *61*, 3962; g) C. Zhou, D. M. Birney, *J. Am. Chem. Soc.* **2002**, *124*, 5231.

[13] Strongly pericyclic transition states often show NICS profiles with values much higher than those reported here and also significantly higher than values found for benzene.

[14] K. Wang, Q. Wu, S. Bi, L. Lui, G. Chen, Y. Li, T. D. James, Y. Liu, *Chem. Commun.* **2021**, *57*, 1494.

[15] M. Castiñeira Reis, M. Marín-Luna, N. Janković, O. Nieto Faza, C. S. López, *J. Catal.* **2020**, *392*, 159.

[16] a) P. Hohenberg, W. Kohn, *Phys. Rev.* **1964**, *136*, B864; b) W. Kohn, L. J. Sham, *Phys. Rev.* **1965**, *140*, A1133.

[17] Y. Zhao, D. G. Truhlar, *Theor. Chem. Acc.* **2008**, *120*, 215.

[18] O. N. Faza, R. Á. Rodríguez, C. S. López, *Theor. Chem. Acc.* **2011**, *128*, 647.

[19] O. N. Faza, C. S. López, *Topics in Current Chemistry*, Vol. 357, Springer, Cham **2015** 213.

[20] R. Bauernschmitt, R. Ahlrichs, *J. Chem. Phys.* **1996**, *104*, 9047.

[21] a) M. Cossi, V. Barone, R. Cammi, J. Tomasi, *Chem. Phys. Lett.* **1996**, *255*, 327; b) B. Mennucci, J. Tomasi, *J. Chem. Phys.* **1997**, *106*, 5151; c) J. Tomasi, B. Mennucci, R. Cammi, *Chem. Rev.* **2005**, *105*, 2999.

[22] D. M. York, M. Karplus, *J. Phys. Chem. A* **1999**, *103*, 11060.

[23] M. J. Frisch, G. W. Trucks, H. B. Schlegel, G. E. Scuseria, M. A. Robb, J. R. Cheeseman, G. Scalmani, V. Barone, G. A. Petersson, H. Nakatsuji, X. Li, M. Caricato, A. Marenich, J. Bloino, B. G. Janesko, R. Gomperts, B. Mennucci, H. P. Hratchian, J. V. Ortiz, A. F. Izmaylov, J. L. Sonnenberg, D. Williams-Young, F. Ding, F. Lipparini, F. Egidi, J. Goings, B. Peng, A. Petrone, T. Henderson, D. Ranasinghe, V. G. Zakrzewski, J. Gao, N. Rega, G. Zheng, W. Liang, M. Hada, M. Ehara, K. Toyota, R. Fukuda, J. Hasegawa, M. Ishida, T. Nakajima, Y. Honda, O. Kitao, H. Nakai, T. Vreven, K. Throssell, J. A. Montgomery Jr., J. E. Peralta, F. Ogliaro, M. Bearpark, J. J. Heyd, E. Brothers, K. N. Kudin, V. N. Staroverov, T. Keith, R. Kobayashi, J. Normand, K. Raghavachari, A. Rendell, J. C. Burant, S. S. Iyengar, J. Tomasi, M. Cossi, J. M. Millam, M. Klene, C. Adamo, R. Cammi, J. W. Ochterski, R. L. Martin, K. Morokuma, O. Farkas, J. B. Foresman, D. J. Fox, *Gaussian 09, Revision E.01*, Gaussian, Inc., Wallingford CT **2016**.

SUPPORTING INFORMATION

Additional supporting information may be found in the online version of the article at the publisher's website.

How to cite this article: I. Stylianakis, I. Litinas, O. Nieto Faza, A. Kolocouris, C. Silva López, *J Phys Org Chem* **2022**, *35*(11), e4333. https://doi.org/10.1002/poc.4333